View metadata, citation and similar papers at core.ac.uk
brought to you by CORE
provided by National Tsing Hua University Institutional Repository

JOURNAL OF APPLIED PHYSICS 99, 053701 (2006)

Magnetic and electrical properties of amorphous CoFeB films

S. U. Jen[a] and Y. D. Yao
Institute of Physics, Academia Sinica, Taipei, Taiwan 11529, Republic of China

Y. T. Chen, J. M. Wu, and C. C. Lee
Department of Materials Science and Engineering, National Tsing-Hua University, Hsinchu, Taiwan 30043, Republic of China

T. L. Tsai
Department of Physics, National Kaohsiung Normal University, Kaohsiung, Taiwan 824, Republic of China

Y. C. Chang
Department of Mechanical Engineering, National Taiwan University of Science and Technology, Taipei, Taiwan 107, Republic of China

(Received 6 April 2005; accepted 23 January 2006; published online 1 March 2006)

CoFeB films were deposited on glass substrate by the sputtering method. From x-ray-diffraction and electron-diffraction-ring patterns, the major phase in the as-deposited CoFeB film is amorphous (or nanocrystalline). However, we could also identify a minor CoFe(110) crystalline phase in the film. We have tried to suppress this crystalline phase by changing the Ar partial pressure (P_{Ar}) during deposition and found that the optimal condition is $P_{\mathrm{Ar}}=5\times10^{-3}$ Torr. Because the electrical resistivity value (ρ) of the film is in general larger than 100 $\mu\Omega$ cm, it also indicates that the amorphous phase is dominant. From the temperature coefficient of resistance measurement, we learn that the amorphous phase in the CoFeB film crystallizes in succession at two higher temperatures (T_{cr1} and T_{cr2}) than the room temperature (RT). Besides the electrical properties, the film thickness (t_f) dependence of saturation magnetization (M_s), saturation magnetostriction (λ_s), and coercivity (H_c) has also been discussed. From the Auger-depth profile analysis, it is found that there is one CoO_x (with $0.4\leqslant x<1$) oxide layer, about 15 Å in thickness, lying on the top surface of the CoFeB film, and another CoO_x oxide layer, about 20 Å, lying near the CoFeB/glass interface. At RT CoO_x is supposed to be paramagnetic. However, due to the proximity effect between CoO_x and CoFeB, the CoO_x layers may become ferromagnetic with the average magnetization M_{ox}. By fitting the M_s data as a function of $(1/t_f)$, we can show that the last conjecture is correct, and M_{ox} is not zero. The CoO_x layer plays an important role on M_s, λ_s, and H_c of the CoFeB films with t_f ranging from 50 to 503 Å. © *2006 American Institute of Physics*. [DOI: 10.1063/1.2174113]

I. INTRODUCTION

The giant magnetoresistance (GMR) or tunneling magnetoresistance (TMR) property of CoFeB materials has attracted extensive attention in recent years.[1–8] The amorphous CoFeB film has high spin polarization, which could lead to a high TMR value at room temperature (RT).[1] Usually, the CoFeB film is taken either as a free layer or as a pinned layer in the magnetic tunneling junction (MTJ), such as CoFeB/$\mathrm{Al_2O_3}$/CoFeB. Therefore, it is important to study the magnetic and electrical properties of the CoFeB film first. All these data are imperative to the junction applications, i.e., useful when designing a magnetic-field sensor, a pressure sensor, a robotics, or a strain gauge.[9]

In this work, we have studied various magnetic and electrical properties, such as saturation magnetization (M_s), saturation magnetostriction (λ_s), coercivity (H_c), and electrical resistivity (ρ) of the CoFeB films. Since all the measurements were performed in the air, a thin layer of CoO_x oxide should form on the top of the CoFeB film. Moreover, according to Auger-depth profile analysis (Fig. 1), the structure of each CoFeB film includes not only a thin layer of CoO_x oxide (with $0.4\leqslant x<1$) on the top surface but also another near the bottom CoFeB/glass interface. As a result, the M_s, λ_s, or H_c data are all affected by this laminated film structure. Further, from the high-temperature electrical resistance study, we find that the CoFeB film crystallizes in two

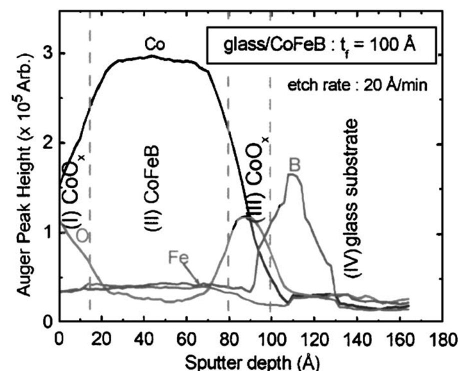

FIG. 1. The CoFeB (t_f=100 Å) film was analyzed by the Auger-depth profile analysis.

[a]Author to whom correspondence should be addressed; FAX: +886-227-834-187; electronic mail: physjen@gate.sinica.edu.tw

Downloaded 19 Dec 2010 to 140.114.66.106. Redistribution subject to AIP license or copyright; see http://jap.aip.org/about/rights_and_permissions

steps.[10] This provides valuable information for the CoFeB-type magnetic sensors, which must sustain under the higher working temperatures than RT.

II. EXPERIMENTS

CoFeB films with the film thickness (t_f) ranging from 25 to 503 Å were deposited by dc magnetron sputtering onto a glass substrate, respectively. The target compositions of CoFeB alloy are 78 at. %Co, 11 at. %Fe, and 11 at. %B. All the CoFeB films were made at RT. The typical base chamber pressure was 2×10^{-7} Torr and the working chamber pressure was 5×10^{-3} Torr. Cross-sectional transmission electron microscopy (XTEM) pictures of several CoFeB films were taken to calibrate the *in situ* Sycon thickness monitor. Then, the thickness (t_f) of each film sample, for later measurements, was read directly from this calibrated thickness monitor.

In order to study the top and bottom interfaces, we did the Auger-depth profile analysis on one CoFeB film sample. The structure of each film was characterized by the x-ray-diffraction method using Cu $K\alpha_1$ line. We also examined a typical CoFeB film by the plane-view TEM. The surface morphology or roughness (S_q) was revealed by an atomic force microscope (AFM). The in-plane magnetic hysteresis loop of each CoFeB film was measured by LakeShore model 7300 vibrating-sample magnetometer (VSM). λ_s was measured by the optical-cantilever method. The details of this method have been described in Refs. 11 and 12. The room-temperature electrical resistivity (ρ) and the high-temperature resistance (R) were measured by the standard four-point-probe method. The temperature coefficient of resistance (TCR) value is defined by the following formula: $\mathrm{TCR}\equiv(1/R)(\Delta R/\Delta T)$, where R is the electrical resistance at temperature T, and ΔR is the resistance difference due to the temperature change ΔT. All the measurements mentioned above, except TCR, were done at RT.

III. RESULTS AND DISCUSSION

In order to study the CoO_x/CoFeB and CoFeB/glass interfaces, a CoFeB film with $t_f=100$ Å has been taken for the Auger-depth profile analysis, as shown in Fig. 1. The ion sputtering rate used in the Auger-depth measurement is assumed to be 20 Å/min, which is actually the rate for SiO_2. The results in Fig. 1 can be divided into four regions: (I) a CoO_x layer on the top, (II) a CoFeB layer in the middle, (III) another CoO_x layer near the CoFeB/glass interface, and (IV) glass substrate, respectively. In region (I), the oxygen concentration C_{O} decreases linearly, while C_{Co} increases linearly. That is, in region (I) x, where $x\equiv C_{\mathrm{O}}/C_{\mathrm{Co}}$, varies roughly from 1 to 0.4 for CoO_x. In region (II), the concentration ratio of $C_{\mathrm{Co}}:C_{\mathrm{Fe}}:\mathrm{C}_B$ is constant and roughly equals to 78:11:11. In region (III), we can also define the second CoO_x layer, where C_{O} and C_{B} increase and then decrease, while C_{Co} decreases only. Once again, the same criterion, $0.4\leq x<1$, has been used to define region (III). Hence, according to this depth profile, the thickness of the outer CoO_x layer (t_{ox}^L) is about 15 Å and that of the inner CoO_x layer (t_{ox}^R) about 20 Å.

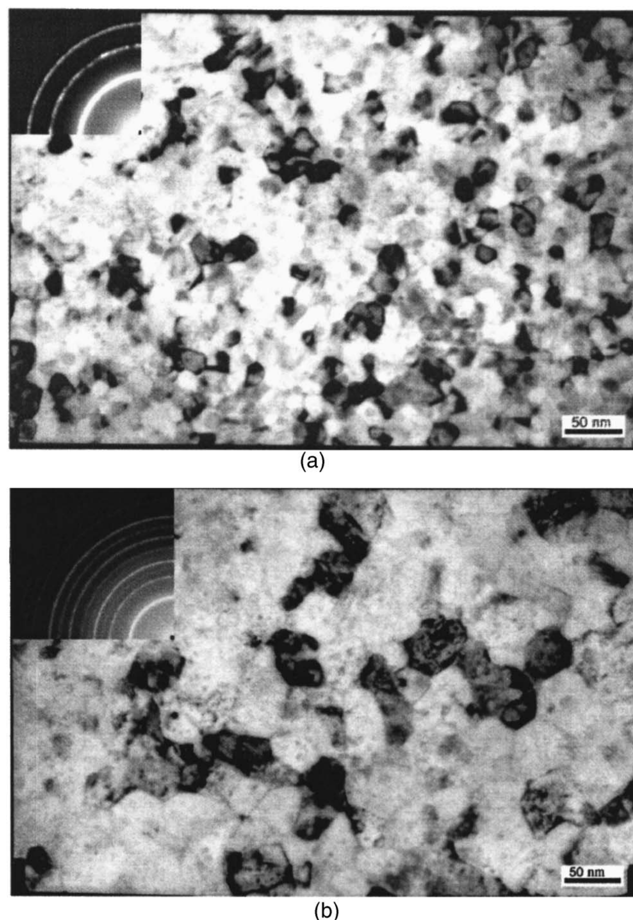

FIG. 2. (a) The as-deposited CoFeB ($t_f=503$ Å) film was observed by the TEM plane view. (b) After TCR measurement the CoFeB ($t_f=503$ Å) film was observed by the TEM plane view again. Each insert shows the corresponding electron diffraction pattern.

The TEM plane-view graph of the as-deposited CoFeB film with $t_f=503$ Å is shown in Fig. 2(a). In this figure, we find that the lateral grain size (D_L) of the amorphous (or nanocrystalline) matrix in the as-deposited CoFeB is as small as 224 Å. Note that it is known that the thickness of the grain (D_T), as determined from the peak broadening of the x-ray-diffraction line, is usually much smaller than the corresponding D_L. Hence, the average grain size ($\bar{D}$), defined as $\bar{D}=(2/3)D_L+(1/3)D_T$, of the as-deposited CoFeB film in Fig. 2(a) must be lower than 224 Å. The insert in Fig. 2(a) shows the electron diffraction pattern of the same film. From this insert, we see that there is a main and broad ring pattern from the amorphous phase, and the other ring patterns, each of which is superimposed on a spot pattern from the crystalline phase. Figure 2(b) shows the TEM plane-view graph of the CoFeB film after the TCR measurement. Apparently, after the thermal cycle of the TCR measurement (up to 200 °C) D_L grows larger and becomes 494 Å. Moreover, from the insert in Fig. 2(b), we discover that the number of the ring patterns has increased a great deal. Therefore, we believe that after the TCR measurement the CoFeB film has been crystallized and its lateral grain size D_L may have increased 2.2 times. In addition, the crystal structure of the as-deposited CoFeB film was analyzed by x-ray diffraction. A typical result is shown in Fig. 3. Besides the high level of the

Downloaded 19 Dec 2010 to 140.114.66.106. Redistribution subject to AIP license or copyright; see http://jap.aip.org/about/rights_and_permissions

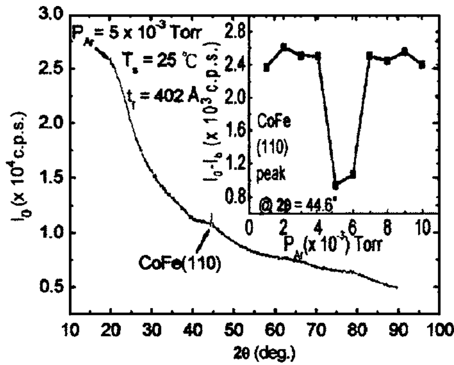

FIG. 3. X-ray measurement of glass/CoFeB 402 Å film was analyzed. The peak shows the existence of the crystalline CoFe(110) phase. I_0 is the absolute intensity. I_b is the background intensity from the amorphous matrix. The insert shows the relationship between the Ar partial pressure during sputtering and the relative intensity of the CoFe(110) peak.

background intensity from the amorphous (or nanocrystalline) phase, we could also identify a small bcc CoFe(110) peak. Once again, it confirms that there are still traces of crystallites coexisting with the amorphous matrix. We have tried to suppress the crystalline phase by varying the Ar pressure (P_{Ar}). The testing results are illustrated in the insert of Fig. 3. Clearly, if the sputtering is done at room temperature $P_{\mathrm{Ar}}=5\times10^{-3}$ Torr is the optimal condition for CoFeB.

The roughness-to-thickness ratio (S_q/t_f) is shown in Fig. 4. It is seen that the S_q/t_f value increases as t_f decreases. These phenomena in general agree with the understanding about the film-growth process, using the sputtering method.

Figure 5 shows the electrical resistivity (ρ) versus film thickness (t_f) plot for the CoFeB film. The results may indicate two things: first, all the ρ values are larger than 100 $\mu\Omega$ cm, which means that the major phase in the CoFeB films is amorphous. This is consistent with the conclusion drawn from the TEM and x-ray studies. Second, ρ increases as t_f decreases. From the ρ vs t_f plot, as shown in Fig. 5, we can summarize the following features: (1) in the range of 50 Å$\leqslant t_f \leqslant$503 Å, ρ increases from 133 to 664 $\mu\Omega$ cm and (2) at t_f=25 Å, ρ becomes very large (up to 5×10^3 $\mu\Omega$ cm). As discussed in Refs. 13–16, the gradual increase of ρ of feature (1) is due to the surface oxidation or roughness effect. However, the sharp increase of ρ of feature (2) must be

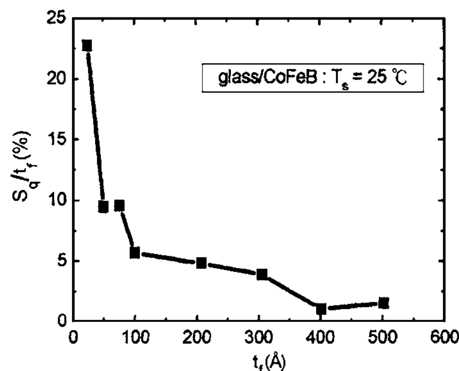

FIG. 4. The surface roughness (S_q) was examined by an AFM. The roughness-to-thickness ratio (S_q/t_f) is a function of CoFeB film thickness (t_f).

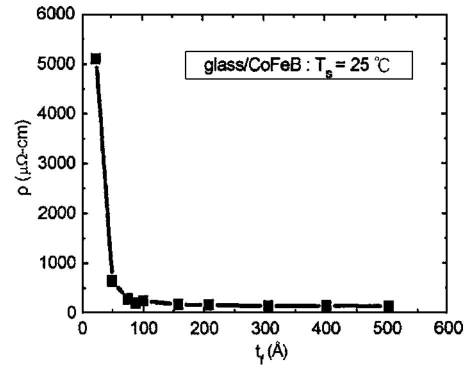

FIG. 5. Electrical resistivity (ρ) plotted as a function of CoFeB thickness (t_f).

due to the fact that the film is at the precoalescence (or discontinuous) stage. The tunneling mechanism,[13] valid for this t_f=25 Å film, explains why ρ is extremely large. Figure 6 shows the TCR plot of one CoFeB film. From this plot, we learn that the crystallization of the CoFeB film occurs in two successive steps: one at the crystallization temperature T_{cr1} =61 °C and the other at T_{cr2}=172 °C. The average TCR value below T_{cr1} is $6.12\times10^{-4}(1/°\mathrm{C})$.

The magnetization (M_s) data of CoFeB films are displayed in Fig. 7. Note that for the CoFeB film with t_f =25 Å, our VSM could only detect the diamagnetic signal from the glass substrate. The reason is twofold. First, the volume of this CoFeB film is much smaller than that of the substrate. Second, the magnetic signal from this CoFeB film is further weakened due to the discontinuous condition of the film. For the CoFeB films with $t_f \geqslant 50$ Å, we had no problems in obtaining their magnetic hysteresis signals and did the substrate correction for each of them. From Fig. 7, we may assume the saturation magnetization of the amorphous CoFeB bulk (M_b^{∞}) to be 1357 G. Further, the Néel temperature (T_N) of bulk CoO is 293 K. Also, T_N of CoO film must be less than that of CoO bulk.[17] Hence, the CoO_x layer in our CoFeB film is supposed to be paramagnetic at RT. However, due to the proximity effect between the CoO_x and CoFeB, the magnetic property of the two CoO_x layers may become ferromagnetic with magnetization M_{ox}. For simplicity we assume the magnetization of the two CoO_x layers to be equal. From previous discussion on the results of Auger-depth analysis, our CoFeB film with thickness t_f is composed of

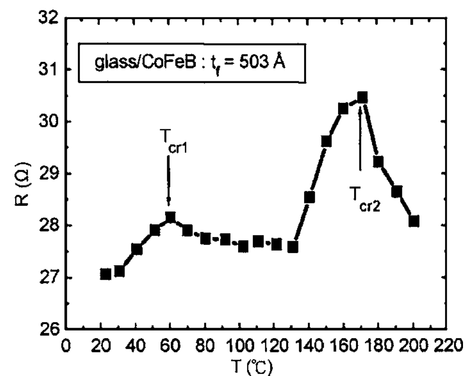

FIG. 6. The TCR electrical properties of the glass/CoFeB(503 Å). (T_{cr1}) and T_{cr2} are the crystallization temperatures.

Downloaded 19 Dec 2010 to 140.114.66.106. Redistribution subject to AIP license or copyright; see http://jap.aip.org/about/rights_and_permissions

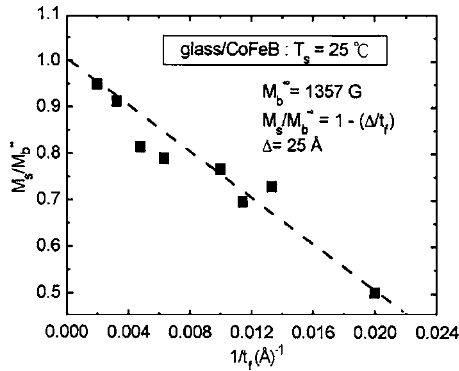

FIG. 7. The saturation magnetization (M_s) was measured by VSM. The M_s/M_b^∞ ratio is plotted as a function of CoFeB film thickness (t_f). M_b^∞ of amorphous CoFeB bulk is equal to 1357 G.

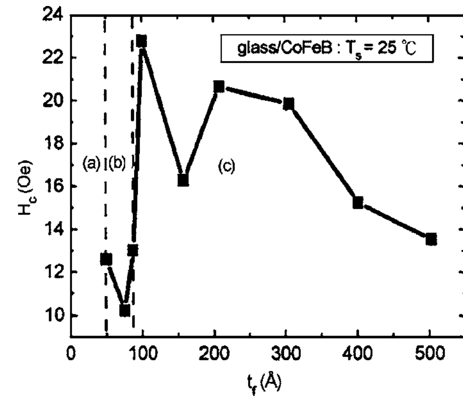

FIG. 9. Coercivity H_c vs the CoFeB film thickness (t_f).

the multilayered structure: (I) an outer CoO_x layer with thickness t_{ox}^L on the top, (II) a CoFeB layer with thickness $(t_f - t_{ox}^L - t_{ox}^R)$ in the middle, and (III) another inner CoO_x layer with thickness t_{ox}^R near the CoFeB/glass interface. Once again, from Fig. 1 we define $t_{ox} = (1/2)(t_{ox}^L + t_{ox}^R) = 17.5$ Å. Then, according to the simple addition rule, the saturation magnetization (M_s) of the CoFeB film can be described as

$$t_f M_s = (t_f - 2t_{ox}) M_b^\infty + 2t_{ox} M_{ox}. \quad (1)$$

From Eq. (1), it is easy to show that

$$M_s/M_b^\infty = 1 - (\Delta/t_f), \quad (2)$$

where $2t_{ox} = \Delta/[1\text{-}(M_{ox}/M_b^\infty)]$. By using Eq. (1) as the fitting equation in Fig. 7 (the dotted line), we find that Δ is 25 Å. Since $t_{ox} = \Delta/2[1\text{-}(M_{ox}/M_b^\infty)]$, it is easy to obtain $M_{ox}/M_b^\infty = 0.29$ or $M_{ox} = 394$ G. This gives a proof to our previous conjecture that the magnetic state of the CoO_x layer is ferromagnetic.

The results of λ_s data are shown in Fig. 8. λ_s of the as-deposited CoFeB film is positive for all the t_f values. In general, the λ_s vs t_f plot in Fig. 8 can be divided into three zones. In zone (A), where $0 < t_f < 50$ Å, the film is discontinuous. We could hardly get any λ_s signal. In zone (B) λ_s increases from 4×10^{-6} to 1×10^{-5}, as t_f decreases from 90 to 50 Å. Finally, in zone (C) λ_s increases from 6.5×10^{-6} to 1.3×10^{-5}, when t_f decreases from 503 to 95 Å. The only way to analyze the λ_s data in zone (C) is by employing the

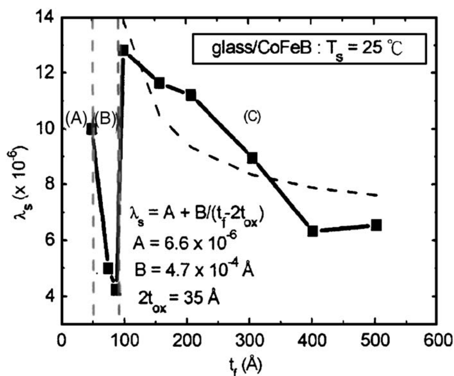

FIG. 8. Magnetostrictions λ_s as a function of CoFeB film thickness. The dash curve in zone (C) is the result based on the Néel formula.

modified Néel model. In this model, in order to treat the CoO_x layers as the surface effect of the CoFeB film, we must set a lower thickness limit (t_0) in describing λ_s. Hence, λ_s is expressed as

$$\lambda_s = A + B/(t_f - t_0), \quad (3)$$

where from our previous discussion $t_0 \equiv 2t_{ox} = 35$ Å, and A and B are fitting constants. As shown in Fig. 8, the dotted curve represents the best fitting result of the λ_s data in zone (C) with Eq. (3). From this fitting, we find $A = 6.6 \times 10^{-6}$ and $B = 4.7 \times 10^{-4}$ Å. Moreover, when crossing over from zone (C) to zone (B), λ_s decreases abruptly at $t_f = t_{fc} \equiv 90$ Å. The reason may be that when $t_f = t_{fc}$ the thickness of CoFeB film is thin enough that the lower boundary of the upper CoO_x layer is about to touch the upper boundary of the inner CoO_x layer. Note, that from Fig. 1, the former (or lower) boundary is about 25 Å below the top surface, and the latter (or upper) boundary is about 40 Å above the glass surface. Here, the thickness of the CoO_y layer (with $0 \leq y \leq 1$) is slightly larger than that of the $CoO_x (0.4 \leq x < 1)$. Therefore, in zone (B) of Fig. 8, we are actually illustrating the λ_s behavior of CoO_x, instead of CoFeB. This is reasonable, since we have shown that the CoO_x film (or layer) is ferromagnetic.

The t_f dependence of H_c of the as-deposited CoFeB film is shown in Fig. 9. This plot can also be divided into three parts. Part (a) in Fig. 9, where $0 < t_f < 50$ Å, corresponds to zone (A) in Fig. 8. As explained before, in this part we could not detect the hysteresis signal from VSM, and therefore H_c is not defined. In part (b), we see the H_c behavior of the CoO_x film (or layer). By using the same criterion, t_{fc} estimated from this set of H_c data is about 88 Å, which agrees with what we found previously from Fig. 8. In part (c), H_c of the CoFeB film roughly increases as $(1/t_f)$ increases. This means that the surface pinning effect, due either to the oxide layer or to the surface roughness, plays a role on H_c. In general, H_c in Fig. 9 is low and in the range of 10–22 Oe. As mentioned previously, the "average grain size" ($\bar{D}$) in the amorphous matrix of the as-deposited CoFeB film is quite small (i.e., $\bar{D} \leq 224$ Å) [Fig. 2(a)]. That means $\bar{D}$ is surely smaller than the exchange length (L_{ex}), which is about 350 Å, for CoFeB. Therefore, the crystalline anisotropy cannot

Downloaded 19 Dec 2010 to 140.114.66.106. Redistribution subject to AIP license or copyright; see http://jap.aip.org/about/rights_and_permissions

be important here.[18] The random anisotropy (over many grains) leads to the consistent result that H_c should be low, as observed in Fig. 9.

IV. CONCLUSION

We have made the $Co_{78}Fe_{11}B_{11}$ films with t_f varied from 25 to 503 Å by the dc sputtering method. From the Auger-depth profile analysis, we could identify one CoO_x layer, about $t_{ox}^L=15$ Å thick, on the top surface of the CoFeB film, and another, about $t_{ox}^R=20$ Å thick, near the CoFeB/glass interface, where x is defined as Co/C_{Co} and $0.4 \leqslant x < 1$. Due to the proximity effect between CoO_x and CoFeB, the CoO_x layer may be ferromagnetic with magnetization M_{ox}. We have proven that the above statement is correct by fitting the M_s data of the CoFeB films with Eq. (2) and found that $M_{ox}=394$ G. From x-ray and TEM measurements, we find that the major phase in the as-deposited CoFeB film is amorphous (or nanocrystalline). However, a minor CoFe(110) crystalline phase also coexists in the film. In order to suppress the crystalline phase, the optimal condition at RT is $P_{Ar}=5\times10^{-3}$ Torr. Since $\rho \geqslant 100\ \mu\Omega$ cm in general, the CoFeB film should contain the amorphous phase mainly. From the TCR measurement, we find that CoFeB film crystallizes in two steps; at $T_{cr1}=61$ °C and $T_{cr2}=172$ °C, respectively. Both the λ_s vs t_f and the H_c vs t_f plots show the two-zone (or two-part) characteristics. The dividing line between zones (B) and (C) for λ_s is at $t_{fc}=90$ Å and that between parts (b) and (c) for H_c is at $t_{fc}=88$ Å. Either in zone (C) or in part (c), we find the λ_s or the H_c behavior of CoFeB, while either in zone (B) or in part (b), we find the λ_s or the H_c behavior of CoO_x.

ACKNOWLEDGMENTS

This work is supported by the National Science Council of Taiwan (NSC94-2120-M-001-004 and NSC94–2112–M001–040). We would like to thank T. C. Wu and S. H. Huang for the assistance in experimental work.

[1] D. Wang, C. Nordman, J. M. Daughton, Z. Qian, and J. Fink, IEEE Trans. Magn. **40**, 2269 (2004).
[2] N. Wiese, T. Dimopoulos, M. Rührig, J. Wecker, H. Brückl, and G. Reiss, J. Magn. Magn. Mater. **290-291**, 1427 (2005).
[3] S. Cardoso, R. Ferreira, P. P. Freitas, M. MacKenzie, J. Chapman, J. O. Ventura, J. B. Sosa, and U. Kressig, IEEE Trans. Magn. **40**, 2272 (2004).
[4] M. Jimbo, K. Komiyama, H. Matue, S. Tsunashima, and S. Uchiyama, Jpn. J. Appl. Phys., Part 2 **34**, L112 (1995).
[5] M. Jimbo, K. Komiyama, Y. Shirota, Y. Fujiwara, S. Tsumashima, and M. Matsuura, J. Magn. Magn. Mater. **165**, 308 (1997).
[6] M. Fujita, K. Yamano, A. Maeda, T. Tanuma, and M. Kume, J. Appl. Phys. **81**, 4909 (1997).
[7] S. Tsunashima, M. Jimbo, Y. Imada, and K. Komiyama, J. Magn. Magn. Mater. **165**, 111 (1997).
[8] T. Feng and J. R. Childress, J. Appl. Phys. **85**, 4937 (1999).
[9] J. Wilson, Sensors, **20**, 19 (2003).
[10] W. Teoh, N. Teoh, and S. Arajs, Amorphous Magnetism, (Plenum, New York, 1977), p. 327.
[11] S. U. Jen, T. C. Wu, C. C. Lin, and K. H. Chang, Solid State Commun. **132**, 259 (2004).
[12] S. U. Jen and C. C. Lin, Thin Solid Films **471**, 281 (2005).
[13] S. U. Jen, C. C. Yu, C. H. Liu, and G. Y. Lee, Thin Solid Films **434**, 316 (2003).
[14] S. U. Jen, T. C. Wu, and C. H. Liu, J. Magn. Magn. Mater. **256**, 54 (2003).
[15] K. L. Chopra, *Thin Film Phenomena* (McGraw-Hill, New York, 1969), Chap. IV.
[16] H. D. Liu, Y. P. Zhao, G. Ramanath, S. P. Muraka, and G. C. Wang, Thin Solid Films **384**, 151 (2001).
[17] T. Ambrose and C. L. Chien, Phys. Rev. Lett. **76**, 1743 (1996).
[18] G. Herzer, IEEE Trans. Magn. **26**, 1397 (1990).

Downloaded 19 Dec 2010 to 140.114.66.106. Redistribution subject to AIP license or copyright; see http://jap.aip.org/about/rights_and_permissions